New Jersey Institute of Technology

Digital Commons @ NJIT

Fall 1-31-1996

Adaptive radar in heterogeneous environment

Albert Futernik
New Jersey Institute of Technology

ABSTRACT

ADAPTIVE RADAR IN HETEROGENEOUS ENVIRONMENT

by
Albert Futernik

Radar performance in heterogeneous clutter has been a much studied topic. In all the studies so far, various forms of the sample matrix inversion (SMI) technique where used to calculate the weight vector of the processor. In this thesis an eigenanalysis-based technique known as the eigencanceler, is used. Performance of this technique is compared to the performance of the generalized likelihood ration (GLR) processor. This comparison is done using the clutter edge model, in which there is an abrupt change in the clutter power in the reference window. It is shown that the false alarm rate fluctuations, of the cell averaging constant false alarm rate (CA-CFAR) eigencanceler, depend on the number of secondary data vectors used to estimate the covariance matrix. It is also shown that when the estimate of the covariance matrix is poor, the eigencanceler is able to perform where the GLR fails.

These two methods are also compared using the range-dependent clutter power model, in which the range clutter power is a Weibull random variable. It is shown that the performance of the eigencanceler depends heavily on the variance of the clutter power random variable. It is again shown that the eigencanceler is able to perform with a low number of range cell samples, where the GLR fails.

ADAPTIVE RADAR IN HETEROGENEOUS ENVIRONMENT

by
Albert Futernik

A Thesis
Submitted to the Faculty of
New Jersey Institute of Technology
in Partial Fulfillment of the Requirements for the Degree of
Master of Science in Electrical Engineering

Department of Electrical and Computer Engineering

Janurary 1996

APPROVAL PAGE

ADAPTIVE RADAR IN HETEROGENEOUS ENVIRONMENT

Albert Futernik

Dr. Alexander Haimovich, Thesis Advisor   Date
Associate Professor of Electrical and Computer Engineering, NJIT

Dr. Hongya Ge, Committee Member   Date
Assistant Professor of Electrical and Computer Engineering, NJIT

Dr. Zoran Siveski, Committee Member   Date
Assistant Professor of Electrical and Computer Engineering, NJIT

BIOGRAPHICAL SKETCH

Author: Albert Futernik

Degree: Master of Science in Electrical Engineering

Date: Janurary 1996

Undergraduate and Graduate Education:

- Master of Science in Electrical Engineering,
  New Jersey Institute of Technology, Newark, NJ, 1996

- Bachelor of Science in Electrical Engineering,
  Rutgers, The State University of New Jersey, College of Engineering, Piscataway,
  NJ, 1994

Major: Electrical Engineering

This work is dedicated to
the memory of my late grandfather, Gregory Goldschmidt

ACKNOWLEDGMENT

I would like to thank my parents for always encouraging me in academics. I would also like to thank Dr. Haimovich for guiding me through my research.

TABLE OF CONTENTS

TABLE OF CONTENTS
(continued)

LIST OF FIGURES

CHAPTER 1

INTRODUCTION

1.1 Previous Work in Adaptive Radar

In airborne radar it is necessary to detect a target in presence of both white Gaussian noise and clutter (colored noise) caused by returns from various obstacles in the terrain. In this situation, the clutter must first be cancelled before detection can take place. To do this, clutter cancellation techniques that adapt to the clutter based on its statistic were developed. Brennan and Reed [1] pioneered the theory of adaptive radar. They derived the optimal linear detector of a known signal in colored Gaussian noise with the covariance matrix known a *priori*. In most practical situations, however, the covariance matrix must be estimated from training data and then updated periodically. This issue was dealt with by Reed, Mallett, and Brennan [19], who suggested the Sample Matrix Inversion (SMI) method in which the covariance matrix is estimated from the secondary data set that does not include the signal of interest. This matrix is then substituted for the actual covariance matrix in the linear detector described in [1]. They showed that in order to achieve performance within 3 dB of the optimal for a signal having dimension M, there has to be about $K = 2M$ samples used in the estimation of the covariance matrix.

1.2 Previous Work with the Eigenanalysis-Based Detector

An alternative way of dealing with clutter is through an eigenanalysis-based approach. A particular version of this method was defined by Haimovich [5]. This technique, known as the eigencanceler, is based on making the weight vector orthogonal to the interference subspace spanned by the eigenvectors corresponding to the first r largest eigenvalues. The behavior of this technique was further studied in [6, 7, 8]. The expressions for probability of detection and false alarm were derived as a of function secondary data length.

Another method using the eigenanalysis was developed by Kirsteins and Tufts [14, 15]. This method is called the principal component inverse (PCI) and, like the eigencanceler, uses the eigenvectors of the covariance matrix to compute the weight vector.

1.3 Previous Work in Non-Stationary Clutter

In [19] it was assumed that the data used to estimate the covariance matrix is stationary with respect to range. If this is not so, performance of a radar system can be effected. In some situations, there may be an abrupt change in the statistics of the clutter, or clutter edge, which makes it difficult for the processor to maintain constant false alarm rate (CFAR). Hansen [10] proposed a method of accomplishing CFAR in a clutter edge region known as the greatest of (GO) CFAR. In this method, the reference window is divided into two parts, before and after the cell-under-test. The threshold is calculated using the side having the largest noise power. In [11] it was shown that this method causes a $0.1 - 0.3$ dB loss in performance relative to the cell averaging (CA) CFAR when operating in a homogeneous environment.

Trunk [23] proposed a method of accomplishing CFAR that prevents the suppression of closely spaced targets. This method, known as the smallest of (SO) CFAR divides the reference window into two parts, before and after cell-under-test. The processor uses the side with the smaller noise power to compute the threshold. Weiss [24] showed that this method causes a performance loss of $0.7 - 11$ dB for $P_f = 10^{-6}$, and when the number of range cells is between $K = 32$ and $K = 4$.

Moore and Lawrence [17] and Weiss [24] further studied these models and showed that if a clutter edge exists in a reference window, and the cell-under-test is in the clutter region of the window, then the threshold is not high enough for the desired false alarm rate. Rohling [20, 21] proposed ordered statistics (OS) CFAR to alleviate the problems associated with GO and SO CFAR. The OS CFAR uses the

n^{th} largest cell in a reference window to estimate the noise power. Finn [3] proposed a heterogeneous clutter estimating (HCE) CFAR. It was shown that this scheme has capabilities that overcome the target masking effects in signal contamination non-homogeneity and false alarm degradation in clutter edge regions.

The non-homogeneity models mentioned above were further studied by Gandhi and Kassam [4]. They performed analyses of different CFAR methods using the clutter edge and signal contamination models. They looked at the OS-CFAR processor, and showed that it works well in the signal contamination non-homogeneity, but not where clutter edge is present. They also looked at the trimmed mean (TM) CFAR processor which at times performed better than the OS-CFAR processor. Wilson [25] described the greatest of order statistics (GOOSE) CFAR and the censored greatest of (CGO) CFAR. He showed that they both work in the signal contamination non-homogeneity and in the presence of clutter edge.

Cai & Wang [2] analyzed the asymptotic, CFAR performance of the generalized likelihood ratio (GLR) test based processor in two types of heterogeneous environments. They described a situation in which there is an abrupt change in the statistics of the clutter and used the clutter edge model to analyze it. They also looked at a scenario where another target is present in the reference window used to estimate the covariance matrix, and used the signal contamination model to analyze it. They showed that given a large support of training data, GLR has the ability to adjust the threshold so that the false alarm rate is fairly constant. They also showed that the performance depends on the width of the clutter spectrum and the target-clutter Doppler separation.

Another heterogeneous clutter model was described by Nitzberg [18] in which the clutter power is a random variable over range. He showed that for this model the estimated covariance matrix does not asymptotically approach the covariance

matrix of the cell-under-test. Szajnowski [22] and Levanon [16] gave properties of the Weibull random variables, which can be used to model the land clutter power.

1.4 Goals

The goal of this thesis is to evaluate performance of the eigencanceler in a heterogeneous environment using the models described above. Comparisons are made between probability of detection and false alarm rate of the eigencanceler and the GLR. The effects of the model parameters, such as the length of the secondary data set, are studied and compared. This is done in order to see if the properties of the eigencanceler alone are capable of dealing with different non-homogeneity scenarios.

CHAPTER 2

ADAPTIVE RADAR

2.1 Formulation of the Problem

Consider the complex envelope of echoes received by a pulsed Doppler radar with M pulse repetition intervals (PRI's) in a coherent processing interval (CPI). Echoes are received from K range cells. Let x be the primary data vector (echoes from the cell-under-test) that consists of M components:

$$\mathbf{x} = (x_1, x_2, \ldots, x_M)^T, \tag{2.1}$$

and let $\mathbf{y}_k$ for $k = 1, 2, \ldots K$ be a set of secondary data vectors corresponding to the K different range cells, as shown in Figure 2.1:

$$\mathbf{y}_k = (y_{1k}, y_{2k}, \ldots, y_{Mk})^T. \tag{2.2}$$

From the above formulation there can be two hypothesis: H_0, target not present; and H_1, target present. For hypothesis H_0, x contains clutter and noise only, i.e.,

$$\mathbf{x} = \mathbf{n}, \tag{2.3}$$

where n has complex Gaussian probability density function (PDF). For H_1, in addition to noise, x contains the target and is given by

$$\mathbf{x} = a\mathbf{s} + \mathbf{n}, \tag{2.4}$$

where a is a zero-mean, Gaussian random variable with circular symmetry and variance σ_s^2. s is the signal vector corresponding to a known velocity of the target having the form

$$\mathbf{s} = \begin{bmatrix} 1 & e^{j2\pi f_s} \ldots e^{j2\pi(M-1)f_s} \end{bmatrix}^T, \tag{2.5}$$

where f_s is the normalized Doppler frequency of the target. The processor has no a *priori* knowledge of the covariance matrix $\mathbf{R} = E[\mathbf{n}\mathbf{n}^H]$ corresponding to n. The
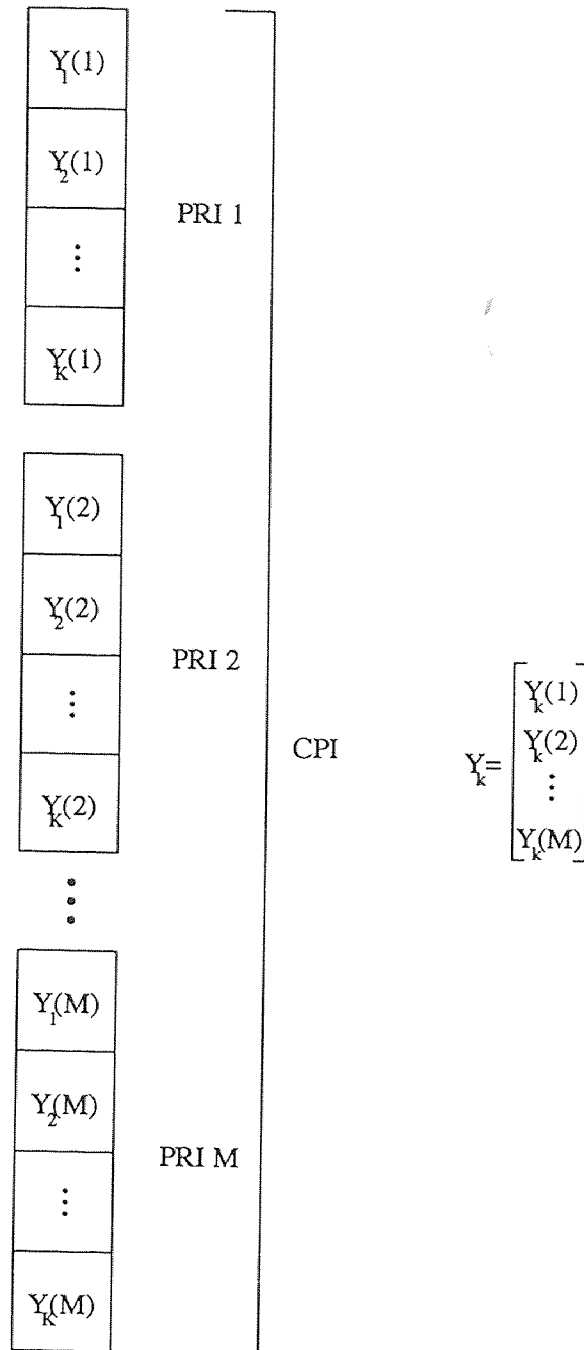
Figure 2.1 Data Model

secondary data vector set y_k is assumed to consist of clutter and noise contributions only, with the same statistics as x, so the covariance matrix can also be written as

$$R = E[yy^H].$$ (2.6)

If the number of range cells K is finite, the covariance matrix can be estimated as [19]

$$\hat{R} = \frac{1}{K} \sum_{k=1}^{K} y_k y_k^H$$ (2.7)

The processor decides on one of the two hypothesis, H_0 or H_1, by taking the instantaneous output power of $w^H x$, where w is the appropriate weight vector as a function of R:

$$\eta = \left| w^H x \right|^2 \underset{H_0}{\overset{H_1}{\underset{<}{>}}} \eta_T,$$ (2.8)

where η_T is the given threshold. The decision statistic η, given a particular w, has an exponential density for both H_0 and H_1.

$$p(\eta/w) = \frac{1}{\bar{\eta}} \exp\left(\frac{-\eta}{\bar{\eta}}\right),$$ (2.9)

where $\bar{\eta}$ is the average output power of the cell-under-test.

$$\bar{\eta} = E[\eta].$$ (2.10)

By integrating the PDF from η_T to ∞ gives the probability of false alarm conditioned on w and H_0:

$$P_{f/w,H_0} = \int_{\eta_T}^{\infty} p(\eta/w)d\eta$$
$$= \exp\left(-\eta_T/\bar{\eta}_{H_0}\right).$$ (2.11)

The probability of detection conditioned on w and H_1 is given by

$$P_{d/w,H_1} = \int_{\eta_T}^{\infty} p(\eta/w)d\eta$$
$$= \exp\left(-\eta_T/\bar{\eta}_{H_1}\right),$$ (2.12)

where $\bar{\eta}_{H_0} = E[\eta/H_0]$ and $\bar{\eta}_{H_1} = E[\eta/H_1]$.
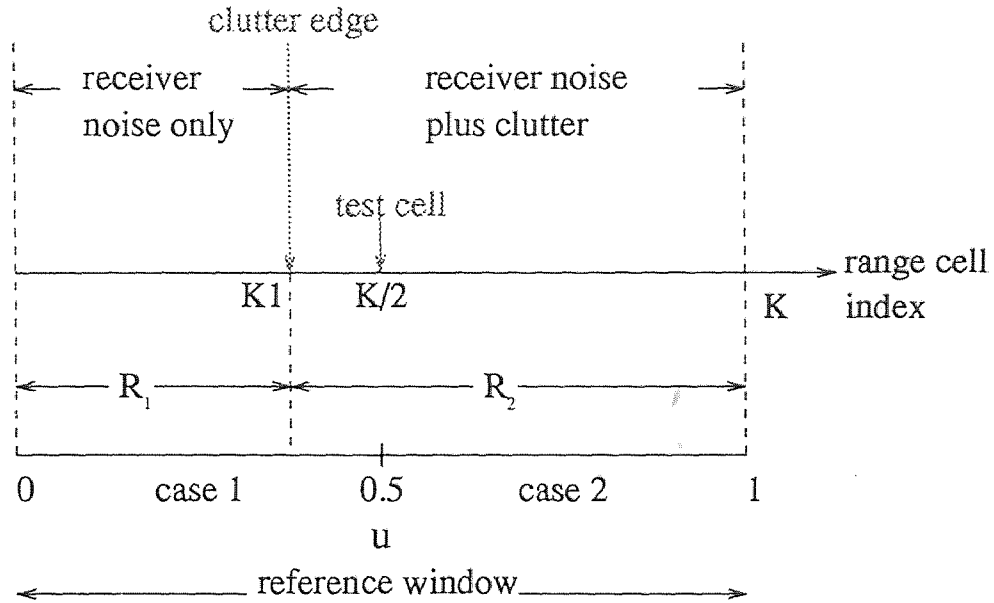
Figure 2.2 Illustration of clutter edge in reference widow.

2.2 Clutter Edge Non-Homogeneity Model

This model, used by Cai and Wang in [2], results from a transition in the clutter across the reference cells as is shown in Figure 2.2. The secondary data set is partitioned into two sets: y_k, $k = 1, 2, \ldots, K_1$ is outside the clutter region and its covariance matrix is denoted by $\mathbf{R}_1$, and y_k, $k = K_1 + 1, \ldots, K$ is within the clutter region and its covariance matrix is $\mathbf{R}_2$.

$$\mathbf{R}_1 = \sigma_v^2 I \tag{2.13}$$

$$\mathbf{R}_2 = \mathbf{R}_c + \sigma_v^2 I, \tag{2.14}$$

where $\mathbf{R}_c$ denotes the covariance matrix of the clutter and has from

$$\mathbf{R}_c = \sigma_c^2 \text{Toeplitz}\{[1 \quad e^{-j2(\pi\sigma_f)^2 - j2\pi f_c} \cdots e^{-j2(\pi\sigma_f(M-1))^2 - j2\pi(M-1)f_c}]\}, \tag{2.15}$$

where σ_c^2 is the clutter power, σ_f is the clutter Doppler spread parameter, and f_c is the center of the clutter spectrum. The power spectral density of the desired signal and the clutter used in our model, are shown in Figure 2.3. A parameter that controls
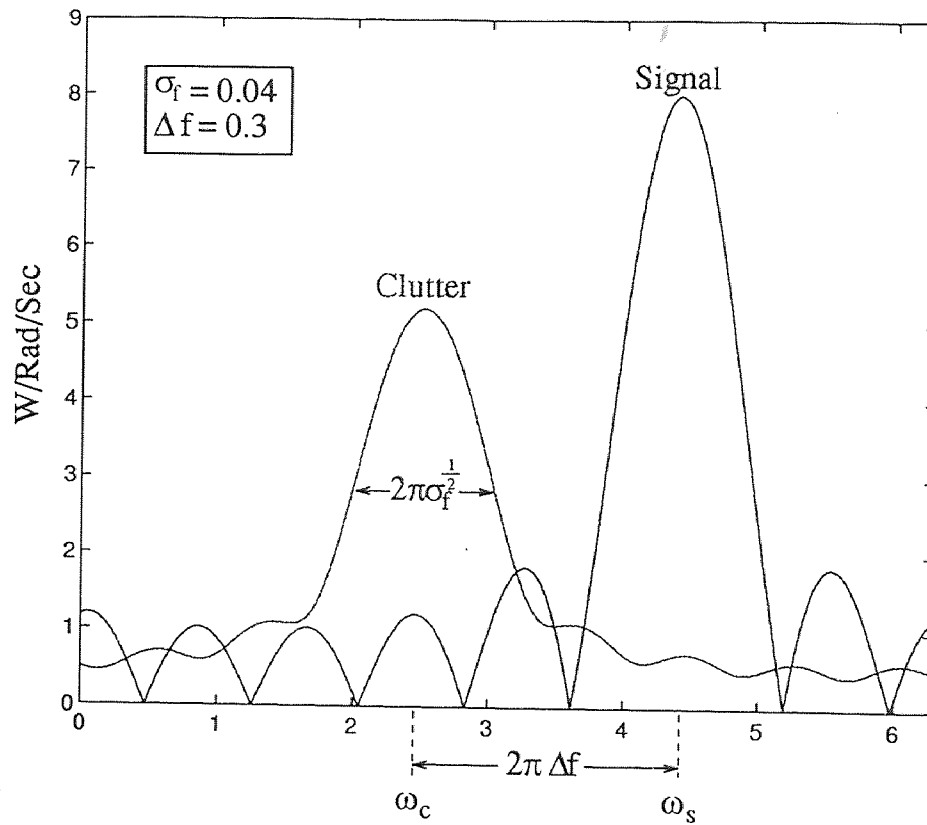
Figure 2.3 PSD of Clutter and Signal

the Doppler separation of the desired signal and the clutter is $\Delta f = f_s - f_c$. The cell-under-test is located at the center of the range.

$$y_1, \ldots, y_{K/2}, x, y_{K/2+1}, \ldots, y_K. \tag{2.16}$$

Denote the parameter $u = K_1/K$ as the "non-homogeneity indicator." Two cases may occur as u varies:

Case 1: The test cell is inside the clutter region if $0 \leq u \leq 0.5$, making $\mathbf{R} = \mathbf{R}_2$.

Case 2: The test cell is outside the clutter region if $0.5 \leq u \leq 1$, making $\mathbf{R} = \mathbf{R}_1$.

As $K \to \infty$, the asymptotic value of the estimated covariance matrix $\hat{\mathbf{R}}$ becomes

$$\lim_{K \to \infty} \hat{\mathbf{R}} = u\mathbf{R}_1 + (1 - u)\mathbf{R}_2. \tag{2.17}$$

This clutter edge model provides a good representation of the real radar data. In particular, it may be applied to some of the Mountain Top data provided by Rome Laboratories. To illustrate the applicability of the model to Mountain Top, the range power is plotted in Figure 2.4. A clutter edge is clearly visible and is indicated.

2.3   Range-Dependent Clutter Power Model

A different model for the heterogeneous can be developed to reflect a case when the clutter power varies as a function of range-time delay [18]. In this model, the complex envelope of each range cell is a zero mean Gaussian random variable with a variance that depends on the reflectivity of the clutter. The reflectivity is a random variable that varies as a function of range. Hence, for this model, the covariance matrix is range dependent:

$$\mathbf{R}(k) = \mathbf{R}_v + P_c(k)\mathbf{R}_c, \tag{2.18}$$

where $\mathbf{R}_v$ and $\mathbf{R}_c$ are the noise and normalized clutter covariance matrices, respectively. $P_c(k)$ is the range dependent clutter power. Numerous clutter models assume
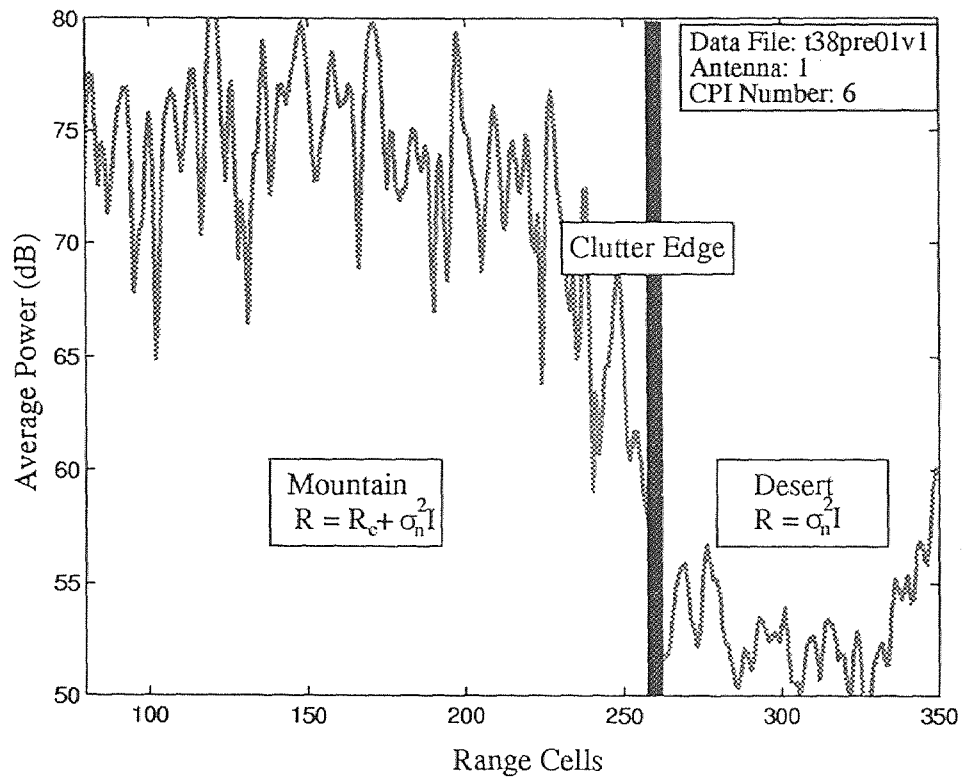
Figure 2.4 Range Power

a Weibull density for the clutter power:

$$p(P_c) = (P_c/q)^{p-1}(p/q) \exp\left[-(P_c/q)^p\right],$$
$$P_c > 0, p > 0, q > 0,$$
(2.19)

where q is a scale parameter and p is the sample parameter [22] [16]. When the covariance matrix is estimated from the training data sequence using Equation (2.7), the asymptotic estimate tends to

$$\hat{\mathbf{R}} = \mathbf{R}_v + \bar{P}_c \mathbf{R}_c,$$
(2.20)

where $\bar{P}_c$ is the average clutter power. Since this equation does not equal Equation (2.18), the solution does not asymptotically approach the optimum for each range cell; therefore performance suffers.

CHAPTER 3

INTERFERENCE CANCELLATION METHODS

3.1 Sample Matrix Inversion (SMI)

The optimum weight vector, for cancelling interference when the covariance matrix of the clutter+noise $\mathbf{R}$, and the desired signal s are known a *priori*, is given by the Weiner equation [1]:

$$\mathbf{w} = \mathbf{R}^{-1}\mathbf{s}. \tag{3.1}$$

This equation can be viewed as a whitening filter followed by a matched filter to the channel and the desired signal [12]. To see that, consider the input $\mathbf{x} = \mathbf{s} + \mathbf{n}$, where n has a known covariance matrix $\mathbf{R}$, n can be written in terms of the covariance matrix as

$$\mathbf{n} = \mathbf{Q}\mathbf{\Lambda}^{1/2}\mathbf{v}, \tag{3.2}$$

where v is a zero mean Gaussian random variable, $\mathbf{Q}$ and $\mathbf{\Lambda}$ are the components of the eigen decomposition of $\mathbf{R}$ such that $\mathbf{R} = \mathbf{Q}\mathbf{\Lambda}\mathbf{Q}^H$. It can easily be seen that $E[\mathbf{n}\mathbf{n}^H] = \mathbf{R}$. When $\mathbf{w}^H$ is multiplied by x the output is

$$
\begin{aligned}
\mathbf{w}^H\mathbf{x} &= \mathbf{s}^H\mathbf{R}^{-1}(\mathbf{s}+\mathbf{n}) \\
&= \mathbf{s}^H\mathbf{Q}\mathbf{\Lambda}^{-1}\mathbf{Q}^H(\mathbf{s}+\mathbf{Q}\mathbf{\Lambda}^{1/2}\mathbf{v}) \\
&= \underbrace{\mathbf{s}^H\mathbf{Q}\mathbf{\Lambda}^{-1/2}}_{\text{MF}}\underbrace{\mathbf{\Lambda}^{-1/2}\mathbf{Q}^H}_{\text{WF}}(\mathbf{s}+\underbrace{\mathbf{Q}\mathbf{\Lambda}^{1/2}\mathbf{v}}_{\text{CN}}) \\
&= \underbrace{\mathbf{s}^H\mathbf{Q}\mathbf{\Lambda}^{-1/2}}_{\text{MF}}(\mathbf{\Lambda}^{-1/2}\mathbf{Q}^H\mathbf{s}+\mathbf{v}).
\end{aligned} \tag{3.3}
$$

The whitening filter (WF) decorrelates the colored noise (CN) and the matched filter (MF) is matched to the desired signal s transformed by the whitening filter.

When the covariance matrix is unknown a *priori*, it has to be estimated from a training data using Equation (2.7). The weight vector is then calculated by substituting Equation (2.7) into Equation (3.1). This method is known as the sample

matrix inversion (SMI). Its performance is dependent on the length of the training data used to estimate the covariance matrix, as shown by Reed, Mallet, and Brennan in [19]. This method converges to the optimum solution when the number of training data samples increases to infinity and the data is IID.

3.2 Eigencanceler

The covariance matrix $\mathbf{R}$ can be decomposed in to its associated eigenvectors and eigenvalues:

$$\mathbf{R} = \mathbf{Q}\mathbf{\Lambda}\mathbf{Q}^H, \tag{3.4}$$

where columns of $\mathbf{Q}$ are the eigenvectors of $\mathbf{R}$ and the diagonal of $\mathbf{\Lambda}$ are the eigenvalues of $\mathbf{R}$. Let $\mathbf{Q}_r$ be the matrix containing eigenvectors that span the interference subspace and $\mathbf{Q}_v$ be the matrix containing the eigenvectors that span the noise. Since these two subspaces are orthogonal, $\mathbf{Q}_r^H \mathbf{Q}_v = 0$, any weight vector in the noise space has the property of cancelling interferences. From this formulation can be defined the weight vector of the *minimum norm eigencanceler* as given in [8]:

$$\mathbf{w} = g\mathbf{Q}_v\mathbf{Q}_v^H\mathbf{s}, \tag{3.5}$$

where g is the gain. Another form can be obtained for this expression by using the identity: $\mathbf{Q}_r\mathbf{Q}_r^H + \mathbf{Q}_v\mathbf{Q}_v^H = \mathbf{I}$:

$$\mathbf{w} = g(\mathbf{I} - \mathbf{Q}_r\mathbf{Q}_r^H)\mathbf{s}. \tag{3.6}$$

3.2.1 Probability of False Alarm and Detection for the Eigencanceler

The P_d and P_f can be expressed in terms of the conditioned signal-to-noise ratio (SNR) as was shown in [9]:

$$\rho = \frac{\gamma_{eig}}{\gamma_{opt}}$$

$$= \frac{|\mathbf{w}^H\mathbf{s}|^2}{\mathbf{w}^H\mathbf{R}\mathbf{w}}\frac{1}{\mathbf{s}^H\mathbf{R}^{-1}\mathbf{s}}, \tag{3.7}$$

where γ_{opt} is the SNR for the optimal case (**R** known). It can be shown that

$$\gamma_{opt} = \mathbf{s}^H \mathbf{R}^{-1} \mathbf{s}$$
$$\equiv \alpha.$$

(3.8)

γ_{eig} is the SNR for a case when the eigencanceler weight vector is used:

$$\gamma_{est} = \frac{\left| \mathbf{w}^H \mathbf{s} \right|^2}{\mathbf{w}^H \mathbf{R} \mathbf{w}}.$$

(3.9)

The conditioned SNR ρ has a PDF:

$$p(\rho) = \left(\frac{K}{2} \right)^{r/2} \frac{\exp K/2}{\Gamma(r/2)} \frac{(1/\rho - 1)^{r/2-1}}{\rho^2} \exp \frac{-K}{2\rho} \quad 0 \le \rho \le 1.$$

(3.10)

where r is the rank of the interference subspace. The derivation of this PDF is given in the appendix and is based on [7]. The average output power under H_0 can be rewritten in terms of ρ for the weight vector having gain $g = (\mathbf{s}^H \mathbf{Q}_v \mathbf{Q}_v^H \mathbf{s})^{-1}$, so that $\mathbf{w}^H \mathbf{s} = 1$.

$$\bar{\eta}_{H_0} = E[\eta/H_0]$$
$$= \mathbf{w}^H \mathbf{R} \mathbf{w}$$
$$= \frac{1}{\rho \alpha}.$$

(3.11)

The average output power under H_1 can also be rewritten in terms of ρ as

$$\bar{\eta}_{H_1} = E[\eta/H_1]$$
$$= \left| \mathbf{w}^H a \mathbf{s} \right|^2 + \mathbf{w}^H \mathbf{R} \mathbf{w}$$
$$= \sigma_s^2 + \frac{1}{\rho \alpha}.$$

(3.12)

Now the probability of detection and the probability of false alarm can also be expressed as conditioned on ρ

$$P_{f/\rho} = \exp\left(-\eta_T / \bar{\eta}_{H_0} \right)$$
$$= \exp\left(-\rho \alpha \eta_T \right)$$

(3.13)

$$P_{d/\rho} = \exp\left(-\eta_T / \bar{\eta}_{H_1} \right)$$
$$= \exp\left(-\rho \alpha \eta_T / (1 + \sigma_s^2 \rho \alpha) \right),$$

(3.14)

where η_T is a preset threshold. The average P_d and P_f are then obtained from

$$P_f = \int_0^1 p(\rho) \exp(-\rho\alpha\eta_T)d\rho \qquad (3.15)$$

$$P_d = \int_0^1 p(\rho) \exp\left(\frac{-\rho\alpha\eta_T}{1 + \sigma_s^2\rho\alpha}\right)d\rho. \qquad (3.16)$$

3.2.2 Constant False Alarm Rate

In a Radar system, it is desirable to have a constant false alarm rate (CFAR). One way to accomplished this is by adding a gain to the weight vector such that the average output power $\bar{\eta}/H_0$ is made constant in range. In this way the false alarm rate depends only on the threshold η_T, as it can be seen from the equation:

$$
\begin{aligned}
P_f \quad &= E[P_{f/\mathbf{w},H_0}] \\
&= E[\exp(-\eta_T/\bar{\eta})] \qquad \text{if } \bar{\eta} \text{ is constant} \\
&= E[\exp(-\eta_T/\text{constant})] \qquad\qquad (3.17) \\
&= \exp(-\eta_T/\text{constant}) \qquad \text{since there are no RV's} \\
&= \text{constant}.
\end{aligned}
$$

This is called the cell averaging (CA) CFAR and needs a range-homogeneous environment in order to work. The eigencanceler can be made CA-CFAR by setting g so that the average output power under H_0 is a constant (independent of the output noise power).

$$
\begin{aligned}
\bar{\eta} \quad &= E[\eta/H_0] \\
&= E[|\mathbf{w}^H\mathbf{x}|^2/H_0] \\
&= \mathbf{w}^H\mathbf{R}\mathbf{w} \qquad\qquad (3.18) \\
&= g^2\mathbf{s}^H\mathbf{Q}_v\mathbf{Q}_v^H\mathbf{R}\mathbf{Q}_v\mathbf{Q}_v^H\mathbf{s} \\
&= \text{constant}.
\end{aligned}
$$

Setting the constant to one and solving for g, yields the CA-CFAR eigencanceler weight vector.

$$\mathbf{w} = \frac{\mathbf{Q}_v\mathbf{Q}_v^H\mathbf{s}}{\sqrt{\mathbf{s}^H\mathbf{Q}_v\mathbf{Q}_v^H\mathbf{R}\mathbf{Q}_v\mathbf{Q}_v^H\mathbf{s}}}. \tag{3.19}$$

In the clutter edge model, cell averaging is not effective because the average clutter power taken over the range is not always equal to the clutter power at the cell-under-test. This will cause the output power under H_0 to fluctuate as a function of the non-homogeneity indicator u, hence the false alarm rate will also fluctuate. It is important to note that CA-CFAR cannot compensate for non-homogeneity effects, since it is derived from the homogeneous assumption. Consequently, the non CA-CFAR version of the eigencanceler is used to evaluate performance.

3.3   Generalized Likelihood Ratio (GLR)

The GLR algorithm is derived by Kelly in [13] from the likelihood ratio test. Given an input vector $\mathbf{x}$, a set of secondary data vectors $\mathbf{y}_k$, and two alternate hypothesis, H_0 and H_1, the likelihood ratio test is as follows:

A hypothesis is true if its joint PDF divided by the PDF of the alternate hypothesis is larger then a preset threshold when the numerator and the denominator are separately maximized over the unknown variables.

$$\frac{\max\limits_{unknowns}\ \{f_1\left(\mathbf{x},\mathbf{y}_1,\mathbf{y}_2,...,\mathbf{y}_K\right)\}}{\max\limits_{unknowns}\ \{f_0\left(\mathbf{x},\mathbf{y}_1,\mathbf{y}_2,...,\mathbf{y}_K\right)\}} > L_0, \tag{3.20}$$

where L_0 is the pre-set threshold. Performing the maximization in Equation (3.20) on the given data model gives

$$\frac{1+\mathbf{x}^H\hat{\mathbf{S}}^{-1}\mathbf{x}}{1+\mathbf{x}^H\hat{\mathbf{R}}_k^{-1}\mathbf{x} - \frac{\left|\mathbf{s}^H\hat{\mathbf{S}}^{-1}\mathbf{x}\right|^2}{\mathbf{s}^H\hat{\mathbf{S}}^{-1}\mathbf{s}}} > L_0, \tag{3.21}$$

where $\hat{\mathbf{S}}$ is defined as

$$\hat{\mathbf{S}} = K\hat{\mathbf{R}} = \sum_{k=1}^{K}\mathbf{y}_k\mathbf{y}_k^H. \tag{3.22}$$

Now, defining $\eta_0 \equiv \frac{L_0-1}{L_0}$, results in the GLR test statistics [13]:

$$\eta = \frac{\left|s^H\hat{S}^{-1}x\right|^2}{s^H\hat{S}^{-1}s\left(1+x^H\hat{S}^{-1}x\right)} \overset{H_1}{\underset{H_0}{\gtrless}} \eta_0, \qquad (3.23)$$

where η_0 is the threshold designed to satisfy the desired false alarm rate as given in [13].

$$\eta_0 = 1 - P_{f0}^{1/(K-M+1)}. \qquad (3.24)$$

3.3.1   Asymptotic False Alarm Rate Performance of the GLR

The decision rule for the GLR can be rewritten by multiplying both sides of Equation (3.23) by K, and substituting Equation (3.22) for $\hat{S}$, so the decision rule becomes

$$\lambda = K\eta = \frac{\left|s^H\hat{R}^{-1}x\right|^2}{s^H\hat{R}^{-1}s\left(1+\frac{1}{K}x^H\hat{R}^{-1}x\right)} \overset{H_1}{\underset{H_0}{\gtrless}} K\eta_0 = \lambda_0. \qquad (3.25)$$

As K approaches infinity $\hat{R}$ converges to a constant matrix:

$$\lim_{K\to\infty}\hat{R} = \hat{R}_\infty, \qquad (3.26)$$

also

$$\lim_{K\to\infty} 1 + \frac{1}{K}x^H\hat{R}^{-1}x = 1, \qquad (3.27)$$

so the asymptotic decision rule becomes

$$\lambda_\infty = \frac{\left|s^H\hat{R}_\infty^{-1}x\right|^2}{s^H\hat{R}_\infty^{-1}s} \overset{H_1}{\underset{H_0}{\gtrless}} = \lambda_{0\infty}. \qquad (3.28)$$

This is the same as the decision rule for SMI with CA-CFAR. The weight vector for CA-CFAR SMI is defined as

$$\hat{w} = \frac{\hat{R}^{-1}s}{\sqrt{s^H\hat{R}^{-1}s}}, \qquad (3.29)$$

which, as K approaches infinity, converges to

$$\lim_{K \to \infty} \hat{\mathbf{w}} = \frac{\hat{\mathbf{R}}_\infty^{-1} \mathbf{s}}{\sqrt{\mathbf{s}^H \hat{\mathbf{R}}_\infty^{-1} \mathbf{s}}} \tag{3.30}$$

so the decision becomes

$$\lambda_\infty = \left| \hat{\mathbf{w}}^H \mathbf{x} \right|^2 \underset{H_0}{\overset{H_1}{\underset{<}{>}}} = \lambda_{0\infty}. \tag{3.31}$$

When the primary data vector $\mathbf{x}$ is complex Gaussian, the instantaneous power λ_∞ has an exponential density given by,

$$p(\lambda) = \frac{1}{\bar{\lambda}_{H_0}} \exp\left(\frac{-\lambda}{\bar{\lambda}_{H_0}}\right), \tag{3.32}$$

where $\bar{\lambda}_{H_0}$ is

$$\bar{\lambda}_{H_0} = \hat{\mathbf{w}}^H \mathbf{R} \hat{\mathbf{w}} \tag{3.33}$$

The probability of false alarm is then calculated by averaging over the values of λ. This result is shown by Cai and Wang in [2].

$$P_f = \int_{\lambda_{0\infty}}^{\infty} p(\lambda) d\lambda = \exp\left(\frac{-\lambda_{0\infty}}{\bar{\lambda}_{H_0}}\right) \tag{3.34}$$

CHAPTER 4

PERFORMANCE ANALYSIS

4.1 Analysis of the Clutter Edge Model

In this section, two sets of analysis are performed. First, the asymptotic expression for the false alarm rate is developed for the eigencanceler. This expression is then matched by a corresponding GLR expression, which is plotted and verified by a simulation. Second, the P_f and P_d are derived for the eigencanceler when the covariance matrix is estimated using finite samples. This is done for case 1, cell-under-test in the clutter, of the clutter-edge model. These analytical results are then compared to the simulations, as explained in a later section.

4.1.1 Asymptotic Case

It was shown that as $K \to \infty$, the estimated covariance matrix becomes

$$
\begin{aligned}
\lim_{K \to \infty} \hat{\mathbf{R}} \ &= u\mathbf{R}_1 + (1-u)\mathbf{R}_2 \\
&\equiv \hat{\mathbf{R}}_\infty.
\end{aligned}
\tag{4.1}
$$

Rewriting this expression and performing eigen-decomposition gives

$$
\begin{aligned}
\hat{\mathbf{R}}_\infty \ &= u\mathbf{R}_1 + (1-u)(\mathbf{R}_1 + \mathbf{R}_c) \\
&= \mathbf{R}_1 + (1-u)\mathbf{R}_c \\
&= \sigma_v^2 \mathbf{I} + (1-u)\mathbf{Q}\mathbf{\Lambda}\mathbf{Q}^H \\
&= \sigma_v^2 \mathbf{Q}\mathbf{I}\mathbf{Q}^H + (1-u)\mathbf{Q}\mathbf{\Lambda}\mathbf{Q}^H \\
&= \mathbf{Q}(\sigma_v^2 \mathbf{I} + (1-u)\mathbf{\Lambda})\mathbf{Q}^H.
\end{aligned}
\tag{4.2}
$$

From the equation above, it can be seen that in the asymptotic case, the eigenvectors become invariant with respect to u, so the eigencanceler weight vector also becomes likewise invariant. Therefore, in the asymptotic case, P_f for the eigencanceler becomes invariant to u:

$$
P_f = \exp\left(\frac{-\eta T}{\bar{\eta}_{H_0}}\right),
\tag{4.3}
$$

20

where $\bar{\eta}_{H_0}$ is

$$\lim_{K\to\infty} \bar{\eta}_{H_0} = E[\eta/H_0]$$

$$= \frac{s^H Q_v Q_v^H R Q_v Q_v^H s}{|s^H Q_v Q_v^H s|^2},$$

(4.4)

where $R = R_2$ for case 1 and $R = R_1$ for case 2.

An equivalent expression for the GLR can be derived by substituting Equation (4.2) into Equation (3.34), giving

$$P_f = \exp\left(\frac{-\lambda_{0\infty}}{\bar{\lambda}_{H_0}}\right)$$

(4.5)

$$\bar{\lambda}_{H_0} = \frac{s^H R_\infty^{-1} R R_\infty^{-1} s}{s^H R_\infty^{-1} s},$$

(4.6)

where

$$R_\infty^{-1} = Q(\sigma_v^2 I + (1-u)\Lambda)^{-1} Q^H,$$

(4.7)

again, where $R = R_2$ for case 1 and $R = R_1$ for case 2. Since u affects the eigenvalues, the false alarm rate of the GLR is also affected. The equations for the asymptotic P_f of the eigencanceler and the GLR are plotted versus u in Figure 4.1. They are also compared to a simulation, in which $K = 400$ and $M = 10$. It can be seen that the simulation points and the analytical expressions agree. As predicted, the eigencanceler's false alarm rate stays constant and the false alarm rate of the GLR fluctuates.

4.1.2   Case One: Cell-Under-Test Inside the Clutter

Consider the case when the non-homogeneity indicator is $0 \leq u \leq 0.5$. When $u = 0$, all the range cells are in the clutter and hence the clutter is homogeneous. Therefore, from Equations (3.15) and (3.16), the probabilities of detection and false alarm depend on the threshold η_T, the optimal SNR γ_{opt}, and the number of range cells K. When $u \neq 0$, the secondary data vector becomes heterogeneous in range. The first $K_1 = uK$ range cells consist of noise only, and the rest $K - K_1$ range cells contain clutter+noise contributions. When the clutter-to-noise ratio (CNR) is high the estimated covariance matrix $\hat{R}$ computed from K range cells, $\sum_{k=1}^{K} yy^H$, becomes
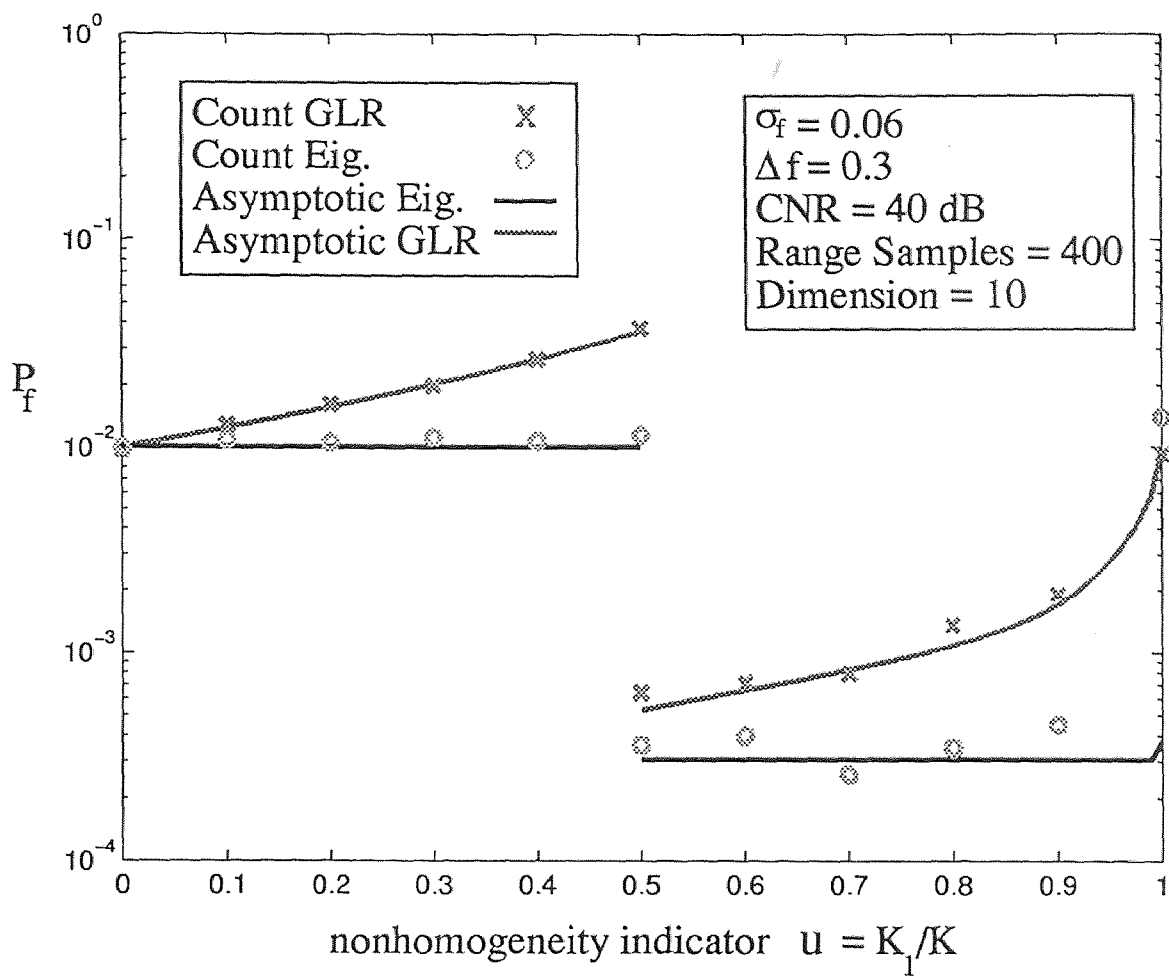
Figure 4.1 Asymptotic False Alarm

almost the same as that computed from the last $K - K_1$ range cells, $\sum_{k=K_1+1}^{K} \mathbf{y}\mathbf{y}^H$, so the effect is the same as reducing K in the homogeneous case. With this observation, Equations (3.15) and (3.16) can still be used to compute probabilities of detection and false alarm by substituting $K - K_1 = K - uK = K(1 - u)$ for K.

$$P_f = \int_0^1 p(\rho) \exp(-\rho \alpha \eta_T) d\rho \tag{4.8}$$

$$P_d = \int_0^1 p(\rho) \exp(\frac{-\rho \alpha \eta_T}{1 + \sigma_s^2 \rho \alpha}) d\rho \tag{4.9}$$

$$p(\rho) = \left(\frac{K(1-u)}{2}\right)^{r/2} \frac{\exp K(1-u)/2}{\Gamma(r/2)} \frac{(1/\rho-1)^{r/2-1}}{\rho^2} \exp \frac{-K(1-u)}{2\rho} \quad 0 \le \rho \le 1 \tag{4.10}$$

$$\alpha = \mathbf{s}^H \mathbf{R}_2 \mathbf{s}. \tag{4.11}$$

Keeping the threshold η_T constant, the above equations show that the probability of false alarm increases from the original desired false alarm rate, as u increases from 0 to 0.5. If the threshold η_T is raised so that the false alarm rate is maintained, then the probability of detection will decrease as accordingly. It is evident that the worst case is at $u = 0.5$, where only half of the samples of the clutter are available to estimate the covariance matrix.

4.1.3 Case Two: Cell-Under-Test Outside the Clutter

For this case the non-homogeneity indicator is $0.5 \le u \le 1$. Since the cell-under-test is outside the clutter, there is no need for clutter cancellation. But, since some of the range cells of the secondary data still contain clutter, the eigencanceler still puts a null in Doppler. This null takes out some of the noise power which has the effect of slightly reducing the false alarm rate. As u increases from 0.5 to 1, this effect decreases and at $u = 1$ the system becomes homogeneous.

4.1.4 Simulation

A set of simulations was carried out to compare the eigencanceler to the GLR under the clutter edge model. Simulated values of the probabilities of detection and false

alarm, as well as the theoretical curves for the eigencanceler, are plotted as a function of u. The simulation involves several steps:

- First N sets of secondary data vectors y_k for $k = 1, 2, \ldots, K$ are generated for a given u:

$$y_k(n) = \begin{cases} \text{noise} & 1 \leq k \leq K_1 \\ \text{clutter+noise} & K_1 + 1 \leq k \leq K \end{cases} \qquad (4.12)$$

$$n = 1, 2, \ldots, N.$$

- Then N covariance matrices are estimated, and their weight vectors are computed:

$$\hat{R}(n) = \frac{1}{K} \sum_{k=1}^{K} y_k(n) y_k^H(n)$$

$$\hat{w}(n) = f(\hat{R}(n)) \qquad (4.13)$$

$$n = 1, 2, \ldots, N.$$

- For each weight vector computed, L data vectors x are simulated under H_0 for the false alarm simulation and under H_1 for the detection simulation:

$$x(n, l) = \begin{cases} \text{clutter+noise} & \text{case 1} \quad H_0 \\ \text{clutter+noise+signal} & \text{case 1} \quad H_1 \\ \text{noise} & \text{case 2} \quad H_0 \\ \text{noise+signal} & \text{case 2} \quad H_1 \end{cases} \qquad (4.14)$$
$$n = 1, 2, \ldots, N$$
$$l = 1, 2, \ldots, L.$$

- The output power η is computed for each run:

$$\eta(n, l) = |w^H(n) x(n, l)|^2. \qquad (4.15)$$

- The output power is put through the decision criterion establishes by Equation (2.8). False alarms and detections are then counted, summed, and divided by NL to obtain the simulated probabilities of false alarm and detection:

$$P_{f-count} = \frac{1}{NL} \sum_{n=1}^{N} \sum_{l=1}^{L} \eta(n,l) | H_0 \geq \eta_T \qquad (4.16)$$

$$P_{d-count} = \frac{1}{NL} \sum_{n=1}^{N} \sum_{l=1}^{L} \eta(n,l) | H_1 \geq \eta_{Td}. \qquad (4.17)$$

- Threshold η_T is set so that at $u = 0$ the probability of false alarm is at a desired level $P_{f-count} = P_{fo}$. This threshold is then kept constant for every u. Threshold η_{Td} is set so that at every u the probability of false alarm is at a desired level $P_{f-count} = P_{fo}$. Therefore it is *different* for every u.

- The output power η is averaged over L runs for each $\mathbf{w}$ and the conditional probabilities are computed using Equations (2.11) and (2.12). These conditional probabilities are then averaged over all the $\mathbf{w}$'s to obtain the simulation/theory probabilities of false alarm and detection:

$$\bar{\eta}(n) = \frac{1}{L} \sum_{l=1}^{L} \eta(n,l) \qquad (4.18)$$

$$P_{f-equation} = \frac{1}{N} \sum_{n=1}^{N} \exp\left(\eta_T / \bar{\eta}(n) | H_0\right) \qquad (4.19)$$

$$P_{d-equation} = \frac{1}{N} \sum_{n=1}^{N} \exp\left(\eta_{Td} / \bar{\eta}(n) | H_1\right). \qquad (4.20)$$

A block diagram of the above description is given in Figure 4.2. The set of thresholds calculated in the simulation for each u, are also used for the theoretical curves, in order to make a fair comparisons. For the GLR method, only the counting simulation is shown, since theoretical expressions for the detection and false alarm probabilities as functions of the secondary data support were not available.

To compare theory and simulation, the secondary data set of the simulation has to have the same covariance matrix as that used in the theoretical calculations.

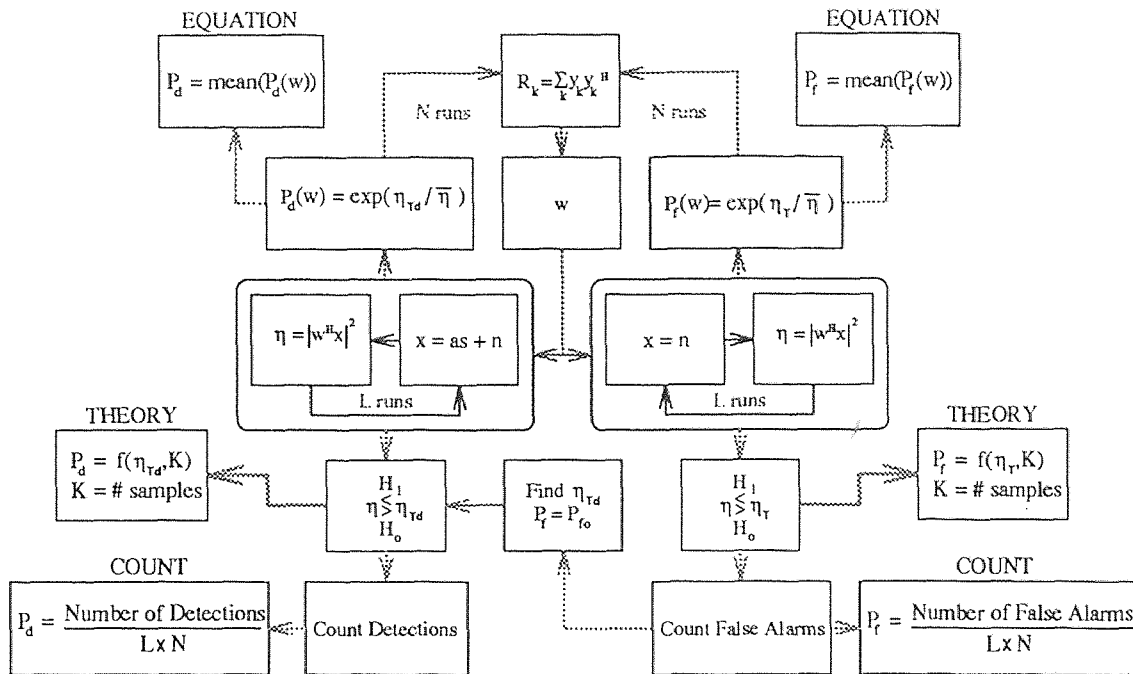$$\mathbf{R} = E\left[\mathbf{y}_k \mathbf{y}_k^H\right]. \qquad (4.21)$$

EQUATION

$P_d = \text{mean}(P_d(w))$

$R_k = \sum_k y_k y_k^H$

N runs   *N runs*

EQUATION

$P_f = \text{mean}(P_f(w))$

$P_d(w) = \exp(\eta_{Td}/\overline{\eta})$

w

$P_f(w) = \exp(\eta_T/\overline{\eta})$

$\eta = |w^H x|^2$ ← $x = as + n$ $x = n$ → $\eta = |w^H x|^2$

L runs   *L runs*

THEORY

$P_d = f(\eta_{Td}, K)$
$K = \#$ samples

H_1
$\eta \gtrless \eta_{Td}$
H_0

Find η_{Td}
$P_f = P_{fo}$

H_1
$\eta \gtrless \eta_T$
H_0

THEORY

$P_f = f(\eta_T, K)$
$K = \#$ samples

COUNT

$P_d = \dfrac{\text{Number of Detections}}{L \times N}$

Count Detections

Count False Alarms

COUNT

$P_f = \dfrac{\text{Number of False Alarms}}{L \times N}$

Figure 4.2 Analysis Method

In order to satisfy the above equation, each secondary data vector was generated from

$$y_k = Q\sqrt{\Lambda}v, \qquad (4.22)$$

where $R = Q\Lambda Q^H$ and v is a zero mean Gaussian random variable with unity variance. Q is a matrix that has eigenvectors of R as its columns and Λ has the eigenvalues of R as its diagonal. Indeed, substituting this definition into the expectation gives

$$
\begin{aligned}
E[y_k y_k^H] &= E\left[Q\sqrt{\Lambda}vv^H\sqrt{\Lambda}Q^H\right] \\
&= Q\sqrt{\Lambda}E\left[vv^H\right]\sqrt{\Lambda}Q^H \\
&= Q\Lambda Q^H \\
&= R,
\end{aligned}
\qquad (4.23)
$$

which is the desired result.

4.1.5 Simulation Results

The simulation described in the previous section is performed for several different parameters. For most of the cases, a covariance matrix of dimension $M = 10$ is used. The CNR is set at $10 \log_{10} \sigma_c^2 / \sigma_v^2 = 20\text{dB}$ and the SNR is set at $10 \log_{10} \sigma_s^2 / \sigma_v^2 = 14\text{dB}$. The Doppler spread parameter is set at $\sigma_f = 0.04$, and the Doppler separation of the desired signal and the clutter is set at $\Delta f = 0.3$. The reason for setting Δf at this value can be seen from Figure 4.3 (a), which shows the projection of the steering vector on the first $r = 4$ eigenvectors as a function of Δf. At $\Delta f = 0.3$, there is a small projection of the first two eigenvectors on s; however, the third and the fourth eigenvectors have a larger one. This means that s is partially in the clutter subspace, so it is necessary to cancel the clutter for the desired signal to be detected. The worst case scenario would be if Δf is equal to 0, in which case the canceler would try to steer a null onto the Doppler frequency of the steering vector s.

Figure 4.3 (b) shows the eigenvalues of the covariance matrix. Based on the figure, the interference subspace was set to $r = 4$ for the simulations concerning the eigencanceler.

Figure 4.4 (a) shows a comparison of false alarm rate as function of u for the eigencanceler counting Equation (4.16), eigencanceler computation Equation (4.19) and the GLR counting for the case where the number of secondary data vectors is low relative to the matrix dimension, $K = M = 10$. It is evident from the plot the close match between the counting and the equation, ($P_{f-count}$ and $P_{f-equation}$). The theoretical curve is derived based on various approximations and while close, it does not provide an accurate estimate of the tail pf PDF, resulting in a low P_f. It can also be seen from the plot that the false alarm rate for the GLR exhibits less variations then the eigencanceler. This is because the eigencanceler is performing a type processing which cannot compensate for clutter heterogeneous effects. The GLR, however, uses the power from the cell-under-test in its decision statistic, and
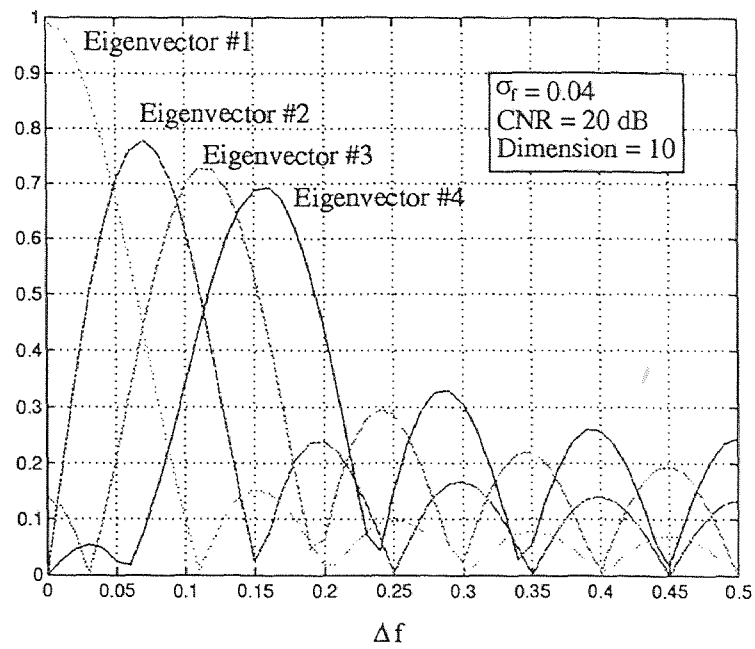
(a)
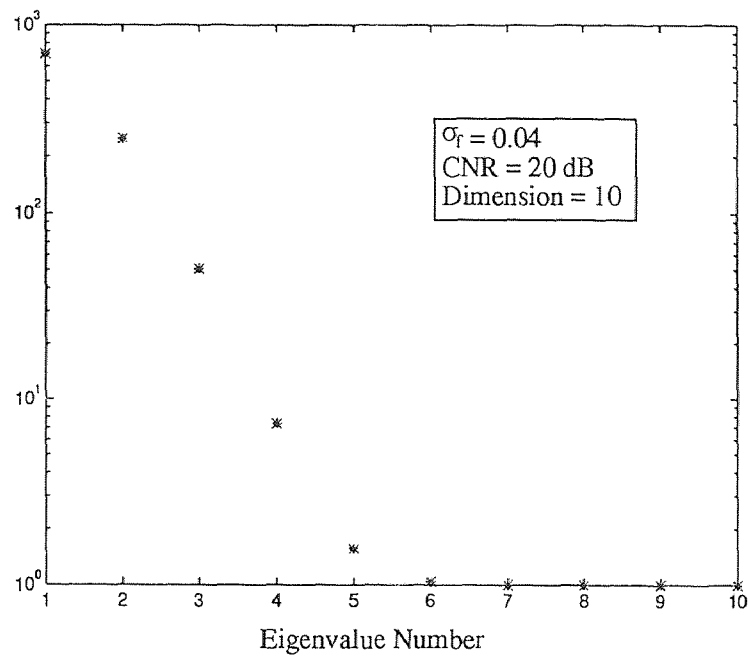
(b)

Figure 4.3 (a) Projections of first $r = 4$ eigenvectors on s. (b) Eigenvalues of R.

this enables compensation for the change in the output power, as described in [2]. Figure 4.4 (b) shows the detection performance comparison. Here, it is evident that the eigencanceler is able to perform where the GLR fails. This is due to the low number of samples in the secondary set.

In Figure 4.5 the number of training samples is increased to $K = 20$. This causes the false alarm rate variations of the eigencanceler to decrease and the detection performance to improve significantly for the GLR and marginally for the eigencanceler. The detection performance of the eigencanceler, however, is still superior to the GLR. The detection performance of the GLR improves dramatically because $K = 2M$. The reason the eigencanceler's false alarm rate fluctuates less evident from the preceding asymptotic analysis. This is further illustrated in Figure 4.6 where $K = 200$. Here, the false alarm rate stays almost constant, as expected.

The performance of the CA-CFAR eigencanceler is shown in Figure 4.7. It can be seen that the false alarm rate is not constant. This is because CA-CFAR eigencanceler was derived assuming homogeneity, which is not the case here. Hence, it fails to keep constant P_f, performing close to the non-CFAR version shown in Figure 4.4

The effect of the clutter Doppler spread parameter Δf is demonstrated in Figure 4.8. Part (a) shows points from the counting simulation for three different values of σ_f. It can be seen that as Δf increases, the false alarm rate has greater variation as a function of u. Part (b) shows detection for the same scenario, with the threshold adjusted so that the false alarm rate is constant. From the plot it can be seen that the effect on detection is proportional to that on the false alarm rate.

Figure 4.9 shows performance for a case when the matrix dimension is increased to $M = 40$, and training data length is $K = 40$. Here again the covariance matrix is ill conditioned, so the GLR fails. When length of the training data is increased
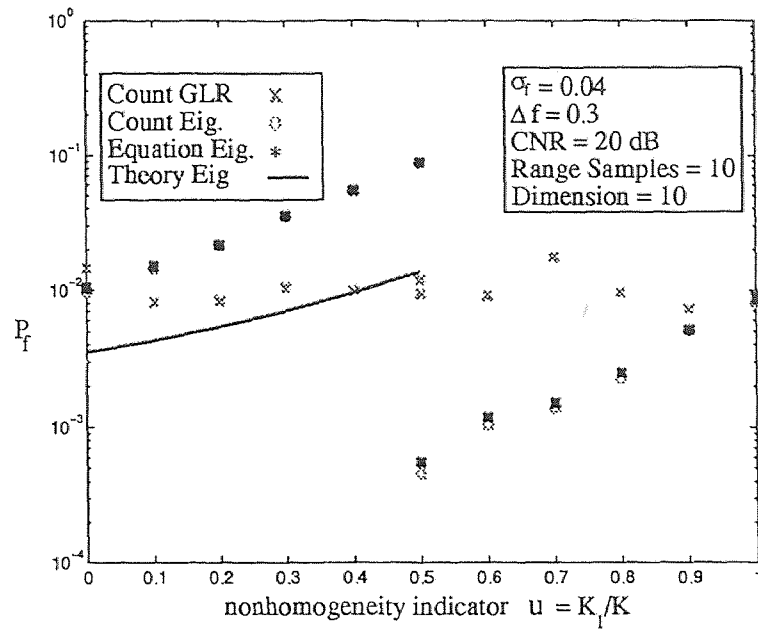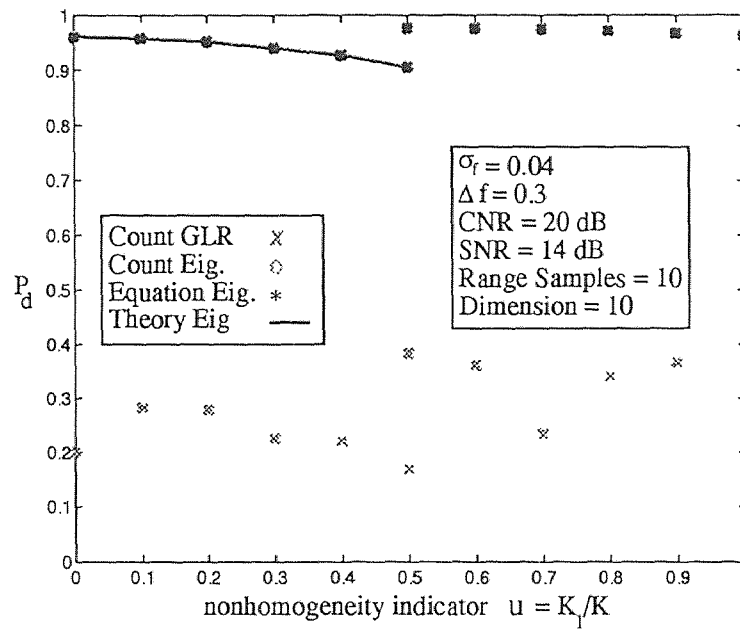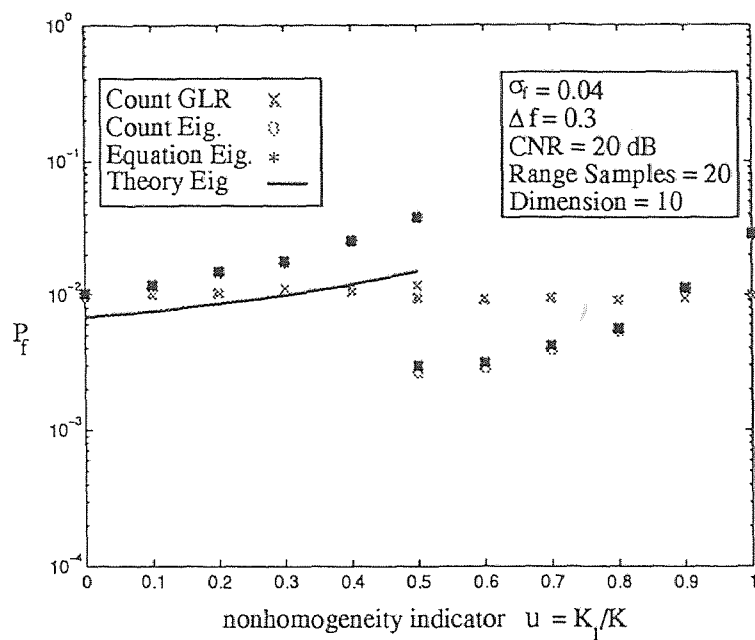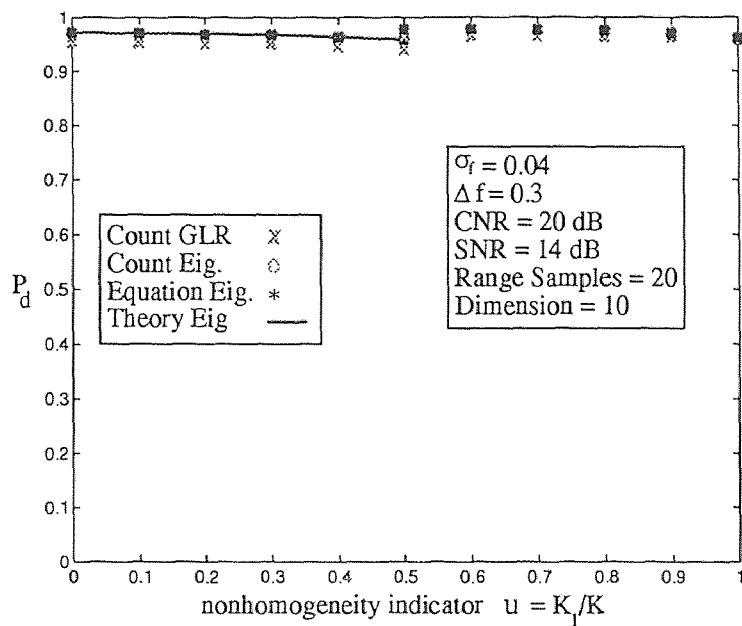
Figure 4.4 (a) False alarm (b) Detection - clutter edge, K = 10.

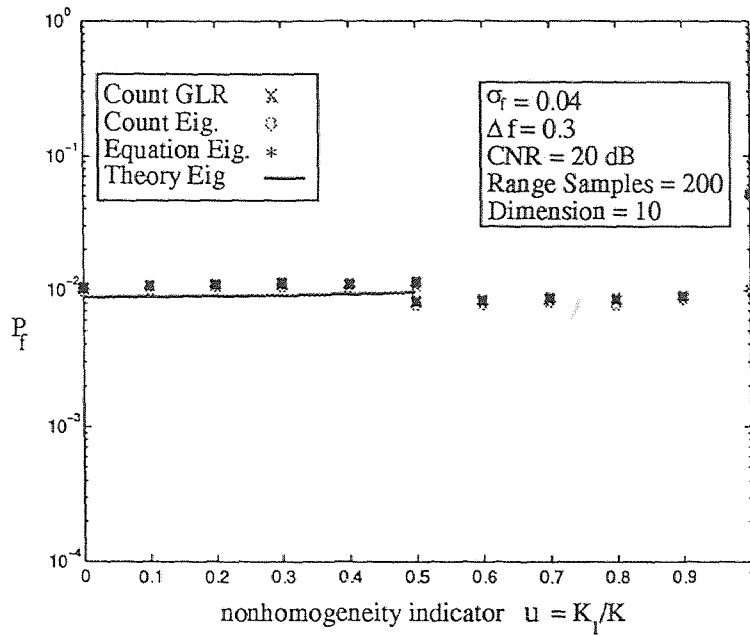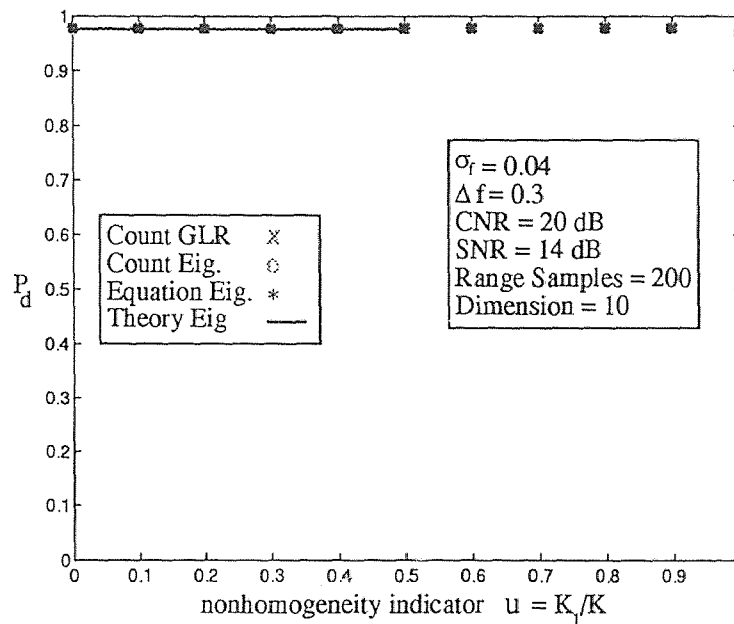**Figure 4.5** (a) False alarm (b) Detection - clutter edge, K = 20.
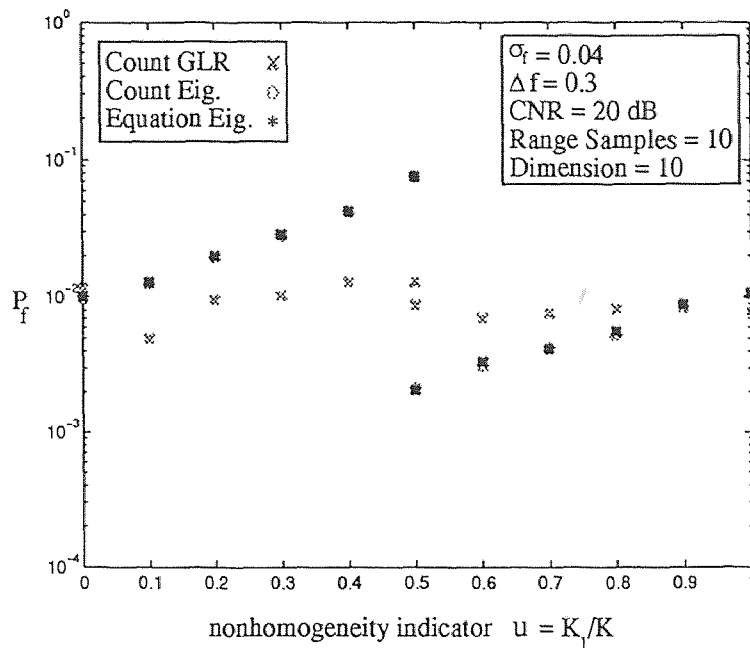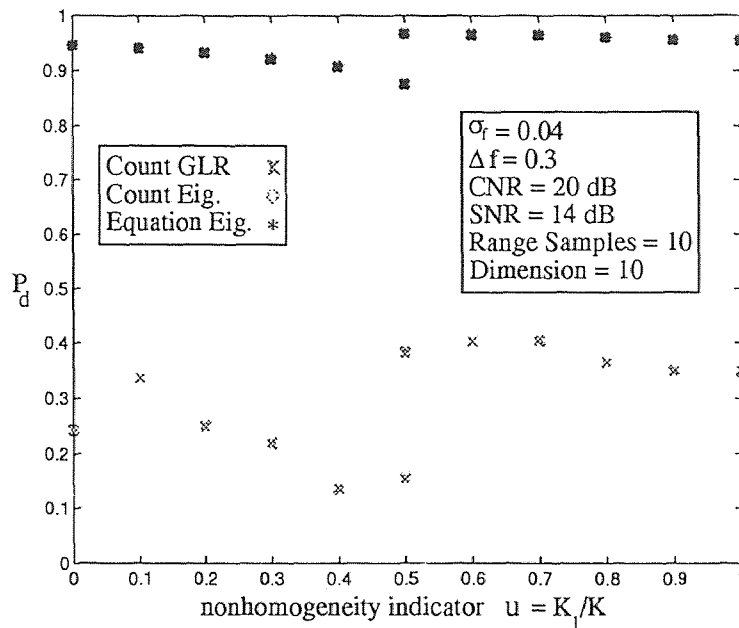
Figure 4.6 (a) False alarm (b) Detection - clutter edge, K = 200.
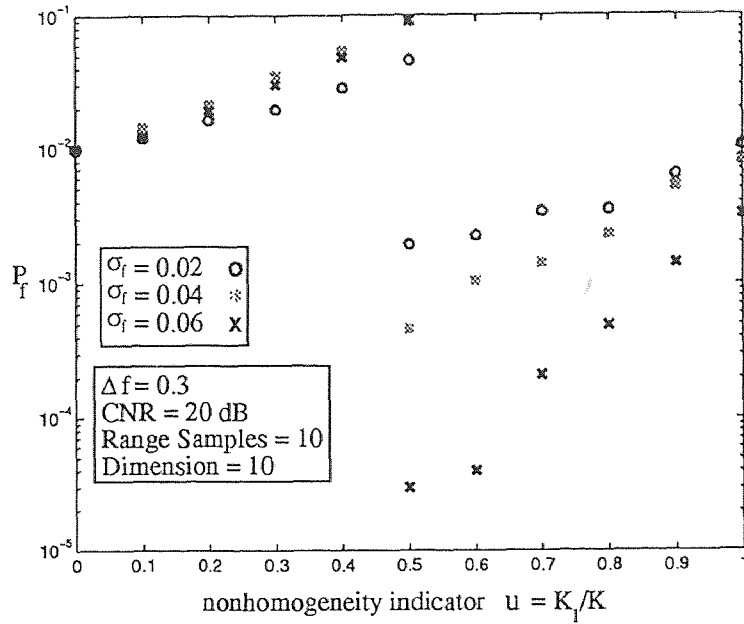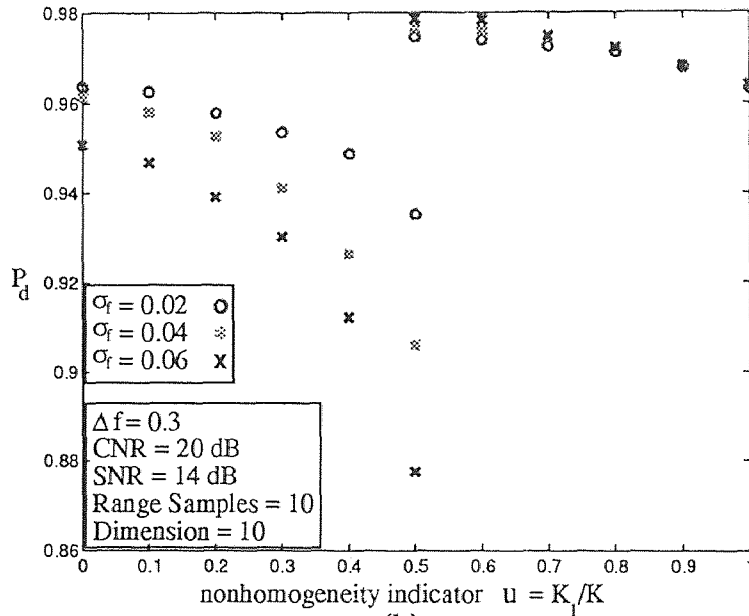
Figure 4.7 (a) False alarm (b) Detection - clutter edge with CFAR eigencanceler.

Figure 4.8 (a) False alarm (b) Detection - clutter edge multiple σ_f using count simulation.

to $K = 80$, the agreement between the theore and simulation is further improved, as can be seen in Figure 4.10. The eigencanceler still outperforms the GLR even though the minimum training data length requirement is met $K = 2M$.

The results described above indicate that the eigencanceler, will in some cases, outperform the SMI-based techniques. For the asymptotic case, the non-homogeneity indicator u, only affects the eigenvalues of the covariance matrix used in inverting the matrix, but not in the eigencanceler. The GLR's capability of keeping its false alarm rate constant is do to its increased complexity of using a compensation from the cell-under-test. SMI, which does not use this compensation, would have been more severely affected by the clutter edge because of the effect of u on the eigenvalues.

4.2   Analysis of the Range-Dependent Clutter Power Model

Analysis of the clutter edge model are performed using a set of simulations with a similar sequence of step as the clutter-edge model. Instead of using u as a non-homogeneity indicator, a variable p is used, which is inversely proportional to the variance of the range-dependent clutter power $P_c(k)$. A Weibull random variable can be generated using two Gaussian random variables as follows [22]:

$$P_c(k) = (X^2(k) + Y^2(k))^{1/p} \quad k = 1, 2, \ldots, K, \qquad (4.24)$$

where X and Y are zero mean Gaussian random variables with variance σ^2. The mean and variance of P_c can be written in terms of p and σ.

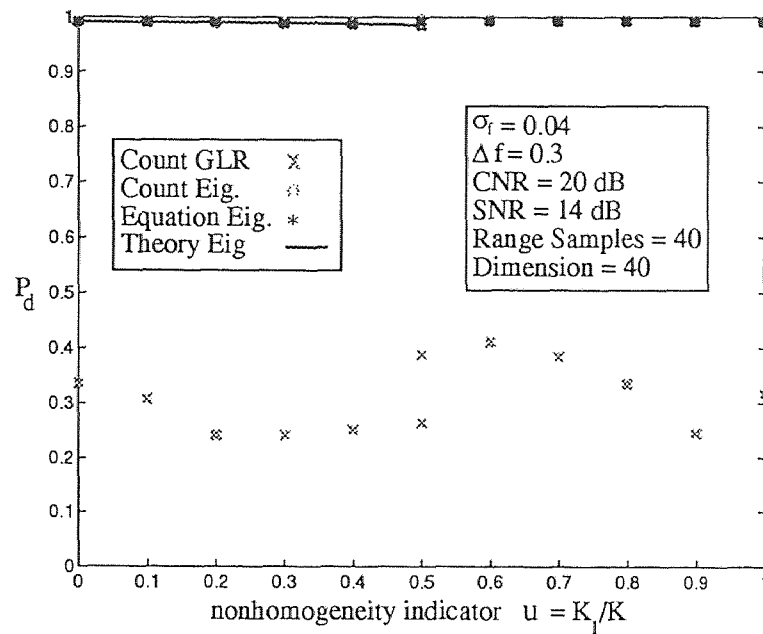$$E[P_c] = (2\sigma^2)^{1/p}\Gamma(1 + 1/p) \qquad (4.25)$$

$$\sigma_{P_c}^2 = (2\sigma^2)^{2/p}[\Gamma(1 + 2/p) - \Gamma^2(1 + 1/p)]. \qquad (4.26)$$

The scale parameter q from the expression of the Weibull PDF can be written as
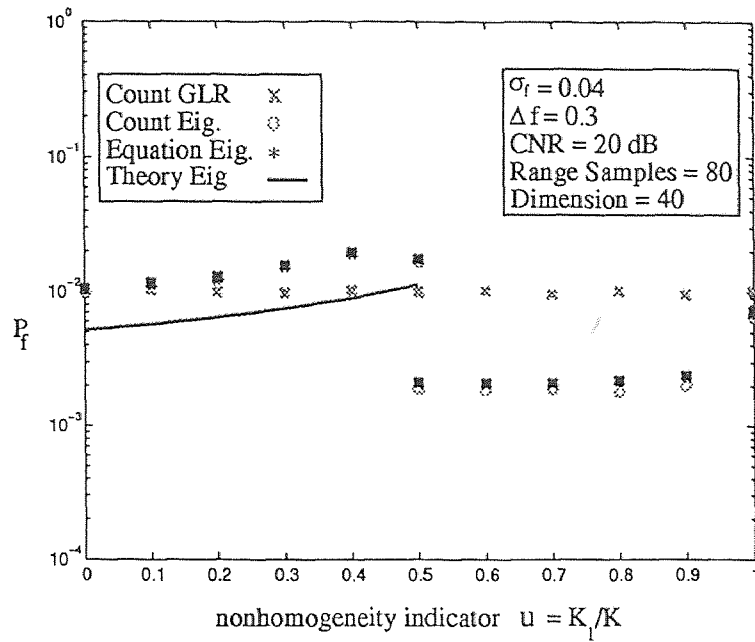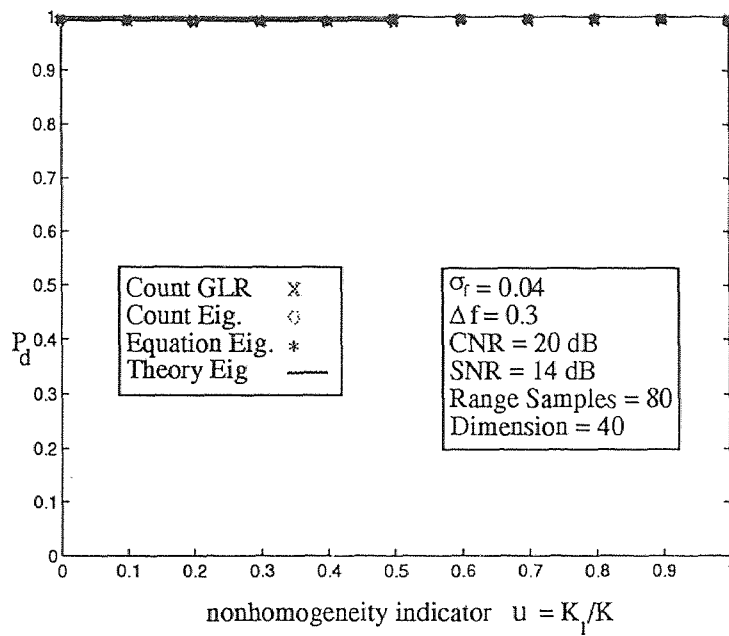
$$q = (2\sigma)^{1/p}. \qquad (4.27)$$
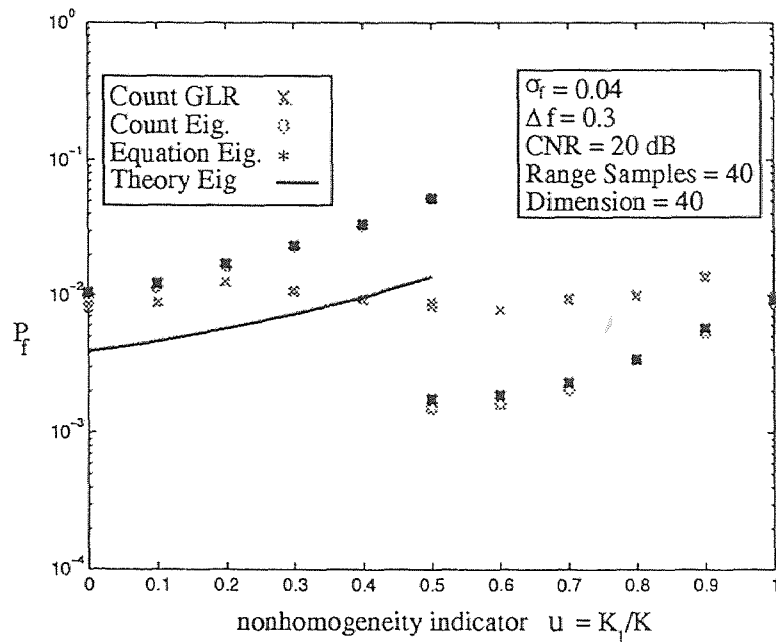
Figure 4.9 (a) False alarm (b) Detection - clutter edge K = 40, M = 40.

Figure 4.10 (a) False alarm (b) Detection - clutter edge K = 80, M = 40.

In the simulations, q is adjusted such that the mean of P_c equals to σ_c^2, maintaining a constant CNR. This is done by solving Equation (4.25) for σ^2 and plugging in $E[P_c] = \sigma_c^2$.

$$\sigma^2 = \frac{1}{2} \left(\frac{\sigma_c^2}{\Gamma(1 + 1/p)} \right)^p \tag{4.28}$$

P_c is calculated for each range cell using the method mentioned above. Cell-under-test has constant clutter power equal to σ_c^2. In Figure 4.11 the probability of detection is plotted as a function of p. As p goes from 0.1 to 2.3, $\sigma_{P_c}^2$ goes from 90 dB to 30 dB. As $\sigma_{P_c}^2$ decreases, variations in P_c decrease, which results in P_c becoming constant-like. This can be seen in Figure 4.11: as p increases, the probability of detection approaches that of the homogeneous case.

This simulation is performed for two training data lengths, $K = 10$ and $K = 20$, shown in Figure 4.11 (a) and (b), respectively. For $K = 10$ the eigencanceler outperforms the GLR for all p. This is not surprising because the GLR, like SMI, needs more secondary data vectors for acceptable performance. Since the dimension of the covariance matrix is $M = 10$, this criteria is not met, and therefore detection performance is very poor. The eigencanceler also fails to detect the target when p is small. This is so because when p is small, the variance of the range dependent clutter power is large, making it look closer to white noise. Therefore, when the clutter is spread in the frequency domain, cancellation by null steering has a lesser effect. As p increases, the null placed by the eigencanceler becomes more effective, and the detection performance approaches the homogeneous case.

For $K = 20$, the GLR has $2M$ secondary data vectors and provides better detection performance. At $p = 0.3$, the eigencanceler's and the GLR's detection performance even out, and for every point after that, the performance becomes the same as for the homogeneous case, with the eigencanceler being slightly better.
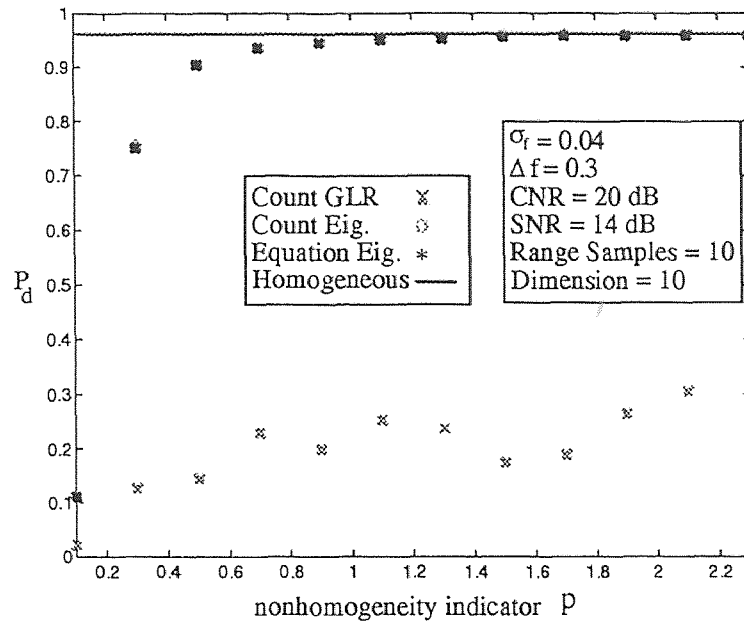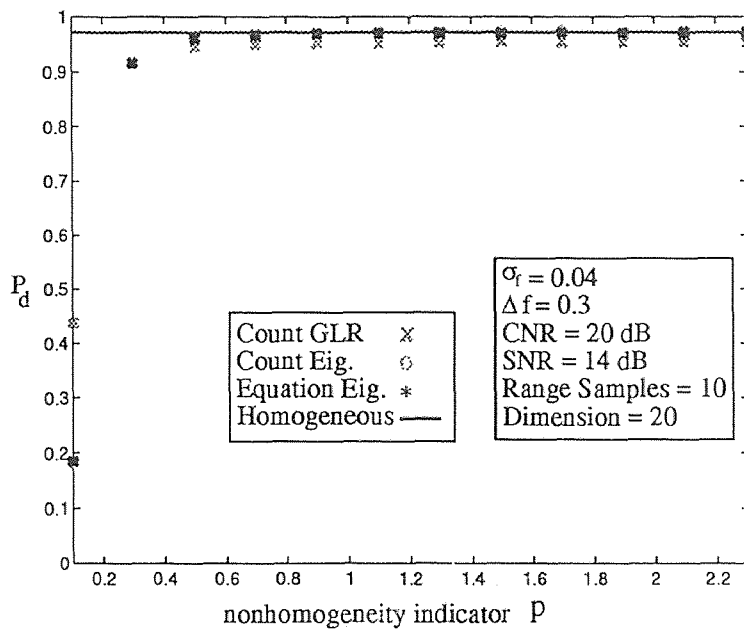
Figure 4.11 Weibull range dependent clutter power

4.3 Summary and Conclusion

In this thesis, performance of the eigencanceler was analyzed and compared to performance of the GLR. It was shown that the eigencanceler outperforms the GLR in the clutter edge model. It was also shown that in the asymptotic case, the non-homogeneity indicator u affects the eigenvalues and not the eigenvectors of the covariance matrix. This makes the eigencanceler a better choice in this situation because it ignores the eigenvalues and only uses the eigenvectors in the computation of the weight vector. Because of this, the deviation of the false alarm rate is reduced by increasing the number of secondary data vectors. This property enables the eigencanceler to be used in an environment where a clutter edge is present without having a serious increase in the false alarm rate when the cell-under-test is in the clutter.

An analytical expression for the clutter edge model was also developed. For the case of cell-under-test in the clutter, it was shown that performance is mainly affected by the number of secondary data vectors with clutter present. This is the same as having a homogeneous case with varying secondary data length, and so the expression for probability of detection and false alarm was derived using this assumption. It is worth noting that the case of target in the clutter is the one of primary interest in the clutter edge model. This is because the false alarm rate increases with u when the cell-under-test is in the clutter. For the case of the cell-under-test outside the clutter, cancellation is not necessary. In this case, the false alarm rate falls below the desired rate, without negative impact on the detection performance, so this effect is not harmful and can be ignored.

The performance of various methods was also evaluated in the range-dependent clutter power model. It was shown that the detection performance of the eigencanceler approaches the level of the homogeneous case as the variance of the clutter power decreases. The performance was improved by increasing the number of secondary data vectors used in the estimation of the covariance matrix. This effect

was considerably more dramatic for the case of GLR then for the eigencanceler. The GLR outperformed the eigencanceler when the variance of the clutter power was extremely high and when the number of the secondary data vectors was sufficiently large. The eigencanceler, however, quickly caught up, and overcame the GLR performance as the variance of the clutter power decreased.

Overall, it can be concluded that the eigencanceler's performance is less affected by a secondary data set that is heterogeneous. This is true for the two models described, as was shown using both simulations and analytical expressions.

APPENDIX A

DERIVATION OF THE PDF FOR THE EIGENCANCELER

It was shown in [7] that the conditioned SNR ρ can be expressed as

$$\rho = g(\zeta) = 1 - \frac{1}{K}\zeta, \tag{A.1}$$

where ζ is a chi-square random variable with r degrees of freedom.

$$p(\zeta) = \frac{1}{2^{r/2}\Gamma(r/2)}\zeta^{r/2-1}\exp\left(-\zeta/2\right)u(\zeta) \tag{A.2}$$

The PDF of ρ can be found using the fundamental theorem of probability:

$$p(\rho) = \frac{p(\zeta_1)}{|g'(\zeta)|}. \tag{A.3}$$

$g'(\zeta)$ is the first derivative of $g(\zeta)$, and ζ_1 is obtained by solving Equation (A.1) for ζ:

$$g'(\zeta) = \frac{-1}{K(1 + \zeta/K)^2} \tag{A.4}$$

$$\zeta_1 = K(1/\rho - 1). \tag{A.5}$$

Plugging these back into Equation (A.3) gives

$$p(\rho) = \begin{cases} \left(\frac{K}{2}\right)^{r/2}\frac{\exp K/2}{\Gamma(r/2)}\frac{(1/\rho-1)^{r/2-1}}{\rho^2}\exp\frac{-K}{2\rho} & 0 \leq \rho \leq 1 \\ 0 & \text{otherwise.} \end{cases} \tag{A.6}$$

REFERENCES

1. L. Brennan and I. Reed, "Theory of adaptive radar," *IEEE Transactions on Aerospace and Electronic Systems*, vol. 9, pp. 237–252, March 1973.

2. L. Cai and H. Wang, "Further results on adaptive filtering with embedded CFAR," *IEEE Transactions on Aerospace and Electronic Systems*, vol. 30, pp. 1009–1020, May 1994.

3. H. Finn, "A CFAR design for a window spanning two clutter fields," *IEEE Transactions on Aerospace and Electronic Systems*, vol. 22, pp. 155–169, March 1986.

4. P. Gandhi and S. Kassam, "Analysis of CFAR processors in nonhomogeneous background," *IEEE Transactions on Aerospace and Electronic Systems*, vol. 24, pp. 427–445, July 1988.

5. A. Haimovich, *Eigenanalysis Techniques for Canceling Narrowband Interferances*, PhD thesis, University of Pennsylvania, 1989.

6. A. Haimovich, "The eigencanceler: a new space-time interference canceler," in *IEEE National Radar Conference*, Atlanta, GA, pp. 194–198, 1994.

7. A. Haimovich, "Asymptotic distribution on the conditioned signal-to-noise ratio in an eigenanalysis-based adaptive array," submitted to *IEEE Transactions on Aerospace and Electronic Systems*, 1995.

8. A. Haimovich, "The eigencanceler: Adaptive radar by eigananlysis method," *IEEE Transactions on Acoustics, Speech, and Signal Processing*, 1996. to appear April.

9. A. Haimovich and M. Berin, "Eigenanalysis-based space-time adaptive radar: Performance analysis," submitted to *IEEE Transactions on Aerospace and Electronic Systems*, 1995.

10. V. Hansen, "Constant false alarm rate processing in search radar," in *IEEE International Radar Conference*, London, England, pp. 325–332, 1973.

11. V. Hansen and J. Sawyers, "Detectability loss due to greatest of selection in cell-averaging CFAR," *IEEE Transactions on Aerospace and Electronic Systems*, vol. 16, pp. 115–118, January 1980.

12. S. Haykin, *Adaptive Filter Theory*, Prentice-Hall, Inc., New Jersey, 1991.

13. E. Kelly, "An adaptive detection algorithm," *IEEE Transactions on Aerospace and Electronic Systems*, vol. 22, pp. 115–127, March 1986.

14. I. Kirsteins and D. Tufts, "Rapidly adaptive nulling of interference," In M. Bouvet and G. Bienvenu (Eds.), *Lecture Notes in Controland Information Sciences*, 1991. New York: Springer-Verlag.

15. I. Kirsteins and D. Tufts, "Adaptive detection using low rank approximation to a data matrix," *IEEE Transactions on Aerospace and Electronic Systems*, vol. 30, pp. 55–67, January 1994.

16. N. Levanon, *Radar Principles*, John Wiley & Sons, New York, 1988.

17. J. Moore and N. Lawrence, "Comparison of two CFAR methods used with square law detection of Swerling I targets," in *IEEE International Radar Conference*, pp. 403–409, 1980.

18. R. Nitzberg, "An effect of range-heterogeneous clutter on adaptive doppler filters," *IEEE Transactions on Aerospace and Electronic Systems*, vol. 26, pp. 475–480, October 1990.

19. I. Reed, J. Mallett, and L. Brennan, "Rapid convergence rates in adaptive arrays," *IEEE Transactions on Aerospace and Electronic Systems*, vol. 10, pp. 853–863, November 1974.

20. H. Rohling, "Radar CFAR thresholding in clutter and multiple target situations," *IEEE Transactions on Aerospace and Electronic Systems*, vol. 19, pp. 608–621, July 1983.

21. H. Rohling, "New CFAR processor based on ordered statistic," in *IEEE International Radar Conference*, Paris, France, pp. 38–42, 1984.

22. W. Szajnowski, "The generation of correlated Weibull clutter for signal detection problems," *IEEE Transactions on Aerospace and Electronic Systems*, vol. 13, pp. 536–540, September 1977.

23. G. Trunk, "Range resolution of targets using automatic detectors," *IEEE Transactions on Aerospace and Electronic Systems*, vol. 14, pp. 750–755, September 1978.

24. M. Weiss, "Analysis of some modified cell-averaging CFAR processors in multiple-target situations," *IEEE Transactions on Aerospace and Electronic Systems*, vol. 18, pp. 102–113, January 1982.

25. S. Wilson, "Two CFAR algorithms for interfering targets and nonhomogeneous clutter," *IEEE Transactions on Aerospace and Electronic Systems*, vol. 29, pp. 57–72, January 1993.